

AN EFFICIENT METHOD FOR THE COMPUTATION OF MIXED POTENTIAL GREEN'S FUNCTIONS IN CYLINDRICALLY STRATIFIED MEDIA

L. F. Ye^{*}, K. Xiao, L. Qiu, S. L. Chai and J. J. Mao

College of Electronic Science and Engineering, National University of Defense Technology, Changsha 410073, China

Abstract—Closed-form mixed potential Green's functions (MPGFs) for cylindrically stratified media are derived in terms of quasistatic-wave and surface-wave contributions. In order to avoid possible overflow/underflow problems in the numerical calculations of special cylindrical functions such as Bessel and Hankel functions, a novel form of the spectral-domain MPGFs is developed. Then, a two-level methodology is used for the approximation of the spectral-domain MPGFs. In the first step, the quasistatic components are extracted from the spectral-domain MPGFs, and then transformed into the space domain with the use of the Sommerfeld identity and its derivatives. In the second step, the remaining parts of the spectral-domain MPGFs are approximated in terms of pole-residue expressions via the rational function fitting method (RFFM). The proposed method is efficient and fully automatic, which avoids an analytical cumbersome extraction of the surface wave poles (SWPs), prior to the spectrum fitting. In addition, this method can evaluate the spatial-domain MPGFs accurately and efficiently for both the near- and far-fields. Finally, numerical results for the spatial-domain MPGFs of a two-layer structure are presented and discussed.

1. INTRODUCTION

Analysis and design of conformal structures play an important role in many practical applications. As a special case of conformal structures, the cylindrically stratified structures have been widely investigated in recent years [1–5].

For the rigorous analysis of printed geometries in cylindrically stratified structures, the method of moments (MoM) is most frequently

Received 23 November 2011, Accepted 10 February 2012, Scheduled 18 February 2012

* Corresponding author: Liang Feng Ye (yeliangfeng2010@hotmail.com).

applied. The MoM procedure can be applied either in the spatial domain or in the spectral domain. as discussed in [13], the spatial domain MoM is considered to be more robust for solving large and complex problem.

The spatial domain MoM, based on the spatial-domain mixed potential Green's functions (MPGFs), are of great interest in the analysis of cylindrical microstrip antennas (Fig. 1) [6–11]. These spatial-domain MPGFs arise in the mixed potential integral equation (MPIE). As well known, the spatial-domain MPGFs can be obtained by computing infinite integrals of the spectral domain counterparts, called Sommerfeld integrals (SIs). Since the integrands are both highly oscillating and slowly converging, the brute-force numerical computation is cumbersome and very time consuming.

In the literature, MPGFs were first developed for single-layered cylindrical structure in [6], The extrapolation and interpolation techniques had been used in [6] to evaluate the summation of cylindrical eigenmodes. However, it only dealt with single-layered structures. Following this development, a more general form of the MPGFs for multilayered cylindrical structure was developed in [11, 12]. In order to improve the convergence behavior of the summation of cylindrical eigenmodes, a new method was proposed in [11–13] for the extraction of the quasi-static components of the spectral domain MPGFs. In this method, the slowly converging quasi-static components were extracted

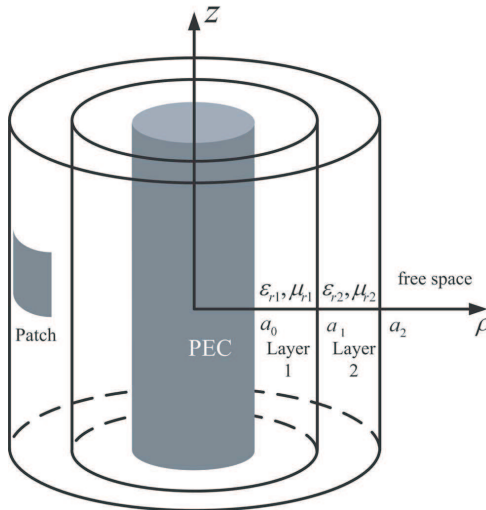


Figure 1. Two-layered cylindrically stratified media with a PEC patch located at the air-dielectric interface.

and then transformed into the space domain analytically. After this extraction, the remaining parts in series became fast convergent and can be easily summed up, then the discrete complex image method (DCIM) with the help of generalized pencil of function (GPOF) method, similar to [14], was applied for obtaining a closed-form solution of the MPGFs in spatial domain. Since the deformed path in [13] can avoid the branch singularity and surface wave pole singularities, there is no need to deal with them explicitly. The method in [13] can provide a very accurate approximation within the range of validity on the order of several wavelengths. However, when distances between the source and field points are beyond several wavelengths where surface-wave contributions become dominant, the extraction of surface wave poles (SWPs) is necessary [11, 15]. To alleviate this problem, a numerical-analytical method was proposed in [7, 16] for extracting the surface-wave contributions explicitly, but since the pole singularities were more complicated than the planar case, this procedure was time consuming. Furthermore, to the best of our knowledge, this method was only restricted to single-layered structure [8, 9].

Recently, a novel approach was proposed for extracting the surface wave poles by the rational function fitting method (RFFM) in the planar stratified media [17–19]. In this approach, the spectrum of the Green's functions was fitted via the RFFM, based on the vector fitting algorithm (VECTFIT) presented in [20, 21], after the extraction of the quasistatic part of the spectrum. Then the spatial domain Green's functions can be expressed in terms of quasistatic-wave and surface-wave contributions with the use of integral identities. Without the process of extracting all the surface-wave poles explicitly, this method was direct and convenient to implement. In [22], this approach was extended to the cylindrically stratified structure. The numerical results obtained for the spatial-domain field Green's functions showed good agreement with the direct numerical results.

The major contribution of this paper is to extend the RFFM method in [22] to the calculation of spatial-domain MPGFs of cylindrically stratified structure. For the sake of consistency, the spectral domain MPGFs for the $e^{j\omega t}$ time convention are derived, which have not yet been found from other published literature. Furthermore, in order to avoid possible overflow/underflow problems in the numerical calculations of special cylindrical functions such as Bessel and Hankel functions, which arise in the MPGFs, a novel form of the spectral-domain MPGFs is developed. Since the infinite series involved converges slowly however, or even diverge, the series acceleration technique should be applied, according to [13]. After the quasistatic parts are completely extracted from the spectral-domain

MPGFs, the RFFM method [22] can be applied for the approximation of the remaining parts. In Section 2, the details of the novel form spectral-domain MPGFs and the approximating RFFM method are presented, In Section 3, some numerical examples of the spatial domain MPGFs are presented for a cylindrically two-layered structure. The numerical results for the spatial-domain MPGFs via the proposed RFFM method are compared with the exact solutions obtained by the direct numerical integrals. Conclusions are summarized in Section 4.

2. THEORY AND FORMULATION

Figure 1 illustrates the geometry for a cylindrically stratified media. The structure is assumed to be infinite in the z -direction. A perfect electric conductor (PEC) forms the innermost region with a radius a_0 , and is surrounded coaxially with two dielectric layers up to radii a_1 and a_2 . The outmost region is free-space. Meanwhile, a PEC patch is printed at the air-dielectric interface. Each dielectric layer has a permittivity and permeability denoted by ε_{rj} , and μ_{rj} , respectively.

Following [14], the spatial domain field Green's functions for cylindrically stratified structure for the $e^{j\omega t}$ time convention can be defined as follows

$$G_{pq}^{E,H}(z-z') = \frac{1}{2\pi} \int_{-\infty}^{\infty} e^{-jk_z(z-z')} \tilde{G}_{pq}^{E,H}(k_z) dk_z \quad (1)$$

where $G_{pq}^{E,H}$ denotes the spatial domain field Green's functions (p , and q can be replaced by z , ϕ , or ρ). $\tilde{G}_{pq}^{E,H}$ denotes the spectral domain field Green's functions, which can be expressed as follows

$$\tilde{G}_{pq}^{E,H} = -\frac{1}{4\omega} \sum_{n=-\infty}^{\infty} e^{jn(\phi-\phi')} \tilde{G}_{pq}^{E_n, H_n}. \quad (2)$$

The complete set of $\tilde{G}_{pq}^{E_n, H_n}$ can be found in the Appendix of [23].

Next, we will derive the spectral-domain MPGFs for the $e^{j\omega t}$ time convention. Similar to [11], the electric field due to the current can be expressed in a mixed potential form as follows

$$\mathbf{E} = -j\omega\mathbf{A} - \nabla\phi \quad (3)$$

where

$$\mathbf{A} = \iint_S \bar{\mathbf{G}}_A \cdot \mathbf{J}(\mathbf{r}') ds' \quad (4)$$

$$\phi = \iint_S \nabla' \cdot \tilde{\mathbf{G}}_\phi \cdot \mathbf{J}(\mathbf{r}') ds'. \quad (5)$$

Note that $\tilde{\tilde{\mathbf{G}}}_E$, $\tilde{\tilde{\mathbf{G}}}_A$, $\tilde{\tilde{\mathbf{G}}}_\phi$ are the spectral domain counterparts of $\bar{\mathbf{G}}_E$, $\bar{\mathbf{G}}_A$, $\bar{\mathbf{G}}_\phi$, respectively, according to [11, 12]

$$\tilde{\tilde{\mathbf{G}}}_E = -j\omega\tilde{\tilde{\mathbf{G}}}_A - \nabla\nabla'(\tilde{\tilde{\mathbf{G}}}_\phi) \quad (6)$$

with

$$\tilde{\tilde{\mathbf{G}}}_E = \begin{bmatrix} \tilde{\tilde{G}}_{\rho\rho}^{E_n} & \tilde{\tilde{G}}_{\rho\phi}^{E_n} & \tilde{\tilde{G}}_{\rho z}^{E_n} \\ \tilde{\tilde{G}}_{\phi\rho}^{E_n} & \tilde{\tilde{G}}_{\phi\phi}^{E_n} & \tilde{\tilde{G}}_{\phi z}^{E_n} \\ \tilde{\tilde{G}}_{z\rho}^{E_n} & \tilde{\tilde{G}}_{z\phi}^{E_n} & \tilde{\tilde{G}}_{zz}^{E_n} \end{bmatrix} \quad (7a)$$

$$\tilde{\tilde{\mathbf{G}}}_A = \begin{bmatrix} \tilde{\tilde{G}}_{\rho\rho}^{A_n} & \tilde{\tilde{G}}_{\rho\phi}^{A_n} & \tilde{\tilde{G}}_{\rho z}^{A_n} \\ \tilde{\tilde{G}}_{\phi\rho}^{A_n} & \tilde{\tilde{G}}_{\phi\phi}^{A_n} & \tilde{\tilde{G}}_{\phi z}^{A_n} \\ \tilde{\tilde{G}}_{z\rho}^{A_n} & \tilde{\tilde{G}}_{z\phi}^{A_n} & \tilde{\tilde{G}}_{zz}^{A_n} \end{bmatrix} \quad (7b)$$

$$\tilde{\tilde{\mathbf{G}}}_\phi = \begin{bmatrix} \tilde{\tilde{G}}_{\rho\rho}^{\phi_n} & 0 & 0 \\ 0 & \tilde{\tilde{G}}_{\phi\phi}^{\phi_n} & 0 \\ 0 & 0 & \tilde{\tilde{G}}_{zz}^{\phi_n} \end{bmatrix} \quad (7c)$$

Following the same procedure and assumptions in [11, 12], we have

$$\begin{cases} \tilde{\tilde{G}}_{zz}^{E_n} = -j\omega\tilde{\tilde{G}}_{zz}^{A_n} - k_z^2\tilde{\tilde{G}}^{\phi_n}, \\ \tilde{\tilde{G}}_{z\phi}^{E_n} = -j\omega\tilde{\tilde{G}}_{z\phi}^{A_n} + \frac{k_z n}{\rho}\tilde{\tilde{G}}^{\phi_n}, \\ \tilde{\tilde{G}}_{\phi z}^{E_n} = -j\omega\tilde{\tilde{G}}_{\phi z}^{A_n} + \frac{k_z n}{\rho'}\tilde{\tilde{G}}^{\phi_n}, \\ \tilde{\tilde{G}}_{\phi\phi}^{E_n} = -j\omega\tilde{\tilde{G}}_{\phi\phi}^{A_n} - \frac{n^2 - 1}{\rho\rho'}\tilde{\tilde{G}}^{\phi_n}. \end{cases} \quad (8)$$

Then let $\tilde{\tilde{G}}_{z\phi}^{A_n} = \tilde{\tilde{G}}_{\phi z}^{A_n} = 0$, the spectral-domain MPGFs can be obtained

$$\tilde{\tilde{G}}^{\phi_n} = \frac{1}{\varepsilon_j} \cdot \left(f_n^{11} + \frac{j\rho\omega\mu_i}{k_z n} \frac{\partial f_n^{21}}{\partial \rho} \right) \quad (9a)$$

$$\tilde{\tilde{G}}_{zz}^{A_n} = \frac{j}{\varepsilon_j \omega} \cdot \left(k_i^2 f_n^{11} + \frac{j\rho\omega\mu_i k_z}{n} \frac{\partial f_n^{21}}{\partial \rho} \right) \quad (9b)$$

$$\begin{aligned} \tilde{\tilde{G}}_{\phi\phi}^{A_n} = & \frac{j}{\varepsilon_j \omega k_{\rho_i}^2} \cdot \left\{ k_j^2 \left(\frac{n^2 f_n^{11}}{\rho\rho'} + \frac{jn\omega\mu_i}{\rho'k_z} \frac{\partial f_n^{21}}{\partial \rho} \right) \right. \\ & \left. - j\omega\varepsilon_j \left(\frac{nk_z}{\rho} \frac{\partial f_n^{12}}{\partial \rho'} + j\omega\mu_i \frac{\partial^2 f_n^{22}}{\partial \rho \partial \rho'} \right) \right\} - \frac{j}{\varepsilon_j \omega \rho \rho'} \cdot \left(f_n^{11} + \frac{j\rho\omega\mu_i}{nk_z} \frac{\partial f_n^{21}}{\partial \rho} \right). \end{aligned} \quad (9c)$$

In the above, f_n^{11} , f_n^{12} , f_n^{21} , and f_n^{22} are the entries of \bar{F}_n , which is a 2×2 matrix given by [15]

$$\bar{F}_n = H_n^{(2)}(k_{\rho_j}\rho)J_n(k_{\rho_j}\rho') \left[\bar{I} + \frac{J_n(k_{\rho_j}\rho)}{H_n^{(2)}(k_{\rho_j}\rho)} \tilde{\mathbf{R}}_{j,j+1} \right] \\ \tilde{\mathbf{M}}_{j+} \left[\bar{I} + \frac{H_n^{(2)}(k_{\rho_j}\rho')}{J_n(k_{\rho_j}\rho')} \tilde{\mathbf{R}}_{j,j-1} \right] \quad (10)$$

where $k_{\rho_j} = \sqrt{k_j^2 - k_z^2}$, with k_j being the wave number of layer j .

Note that Equations (9a)–(9c) are now derived for the $e^{j\omega t}$ time dependence. In addition, in the above expressions, ρ and ρ' are kept distinct, according to [15].

For the sake of derivation's convenience, Equation (9c) can be split into three terms

$$\tilde{G}_{\phi\phi}^{A_n} = \tilde{G}_{\phi\phi}^{Aa_n} + \tilde{G}_{\phi\phi}^{Ab_n} + \tilde{G}_{\phi\phi}^{Ac_n} \quad (11)$$

where

$$\tilde{G}_{\phi\phi}^{Aa_n} = \frac{jk_j^2}{\varepsilon_j\omega k_{\rho_i}^2} \cdot \left(\frac{n^2 f_n^{11}}{\rho\rho'} + \frac{jn\omega\mu_i}{\rho'k_z} \frac{\partial f_n^{21}}{\partial\rho} \right) + \frac{1}{k_{\rho_i}^2} \cdot \frac{nk_z}{\rho} \frac{\partial f_n^{12}}{\partial\rho'} \quad (12a)$$

$$\tilde{G}_{\phi\phi}^{Ab_n} = \frac{1}{k_{\rho_i}^2} j\omega\mu_i \frac{\partial^2 f_n^{22}}{\partial\rho\partial\rho'} \quad (12b)$$

$$\tilde{G}_{\phi\phi}^{Ac_n} = -\frac{j}{\varepsilon_j\omega\rho\rho'} \cdot \left(f_n^{11} + \frac{j\rho\omega\mu_i}{nk_z} \frac{\partial f_n^{21}}{\partial\rho} \right). \quad (12c)$$

Then (9a)–(9b), and (12a)–(12c) can be modified for $\rho = \rho'$ case and rewritten in the following forms

$$\tilde{G}_u^m = \left[\left(\frac{\partial^2}{k_{\rho_j}^2 \partial\rho\partial\rho'} \right)^q \left(H_n^{(2)}(k_{\rho_j}\rho)J_n(k_{\rho_j}\rho') \right) \right] \left[(n/k_{\rho_j})^p \times f_u(n, k_z) \right] \quad (13)$$

where \tilde{G}_u^m stands for $\tilde{G}^{\phi n}$, $\tilde{G}_{zz}^{A_n}$, $\tilde{G}_{\phi\phi}^{Aa_n}$, $\tilde{G}_{\phi\phi}^{Ab_n}$ or $\tilde{G}_{\phi\phi}^{Ac_n}$. $q = 0$, $p = 2$ for $\tilde{G}^{\phi n}$, $q = 1$, $p = 0$ for $\tilde{G}_{\phi\phi}^{Ab_n}$, and $q = 0$, $p = 0$, otherwise. The term $f_u(n, k_z)$ can be explicitly given by

$$f^{\phi n}(n, k_z) = \frac{1}{\varepsilon_j} \cdot \left(f_{r1}^{11} + \frac{j\rho\omega\mu_j k_{\rho_j}}{k_z} f_{r2}^{21} \right) \quad (14a)$$

$$f_{zz}^{A_n}(n, k_z) = \frac{j}{\varepsilon_j\omega} \cdot \left(k_j^2 f_{r1}^{11} + j\rho\omega\mu_j k_z k_{\rho_j} f_{r2}^{21} \right) \quad (14b)$$

$$f_{\phi\phi}^{Aa_n}(n, k_z) = \frac{jk_j^2}{\varepsilon_j\omega} \left(\frac{f_{r1}^{11}}{\rho\rho'} + \frac{j\omega\mu_j k_{\rho_j}}{\rho'k_z} f_{r2}^{21} \right) + \frac{k_z k_{\rho_j}}{\rho} f_{r3}^{12} \quad (14c)$$

$$f_{\phi\phi}^{Ab_n}(n, k_z) = j\omega\mu_j f_{r4}^{22} \quad (14d)$$

$$f_{\phi\phi}^{Acn}(n, k_z) = -\frac{j}{\varepsilon_j \omega \rho \rho'} \cdot \left(f_{r1}^{11} + \frac{j \rho \omega \mu_j k_{\rho_j}}{k_z} f_{r2}^{21} \right) \quad (14e)$$

where f_{r1}^{11} , f_{r2}^{21} , f_{r3}^{12} , and f_{r4}^{22} are the corresponding entries of the 2×2 matrix F_{r1} , F_{r2} , F_{r3} , and F_{r4} , which are the same as Equations (6)–(9) in [24].

Referring to (2), the spectral-domain components which are related to \tilde{G}_u^n can be expressed as

$$\tilde{G}_u = -\frac{1}{4\omega} \sum_{n=-\infty}^{\infty} e^{jn(\phi-\phi')} \tilde{G}_u^n \quad (15)$$

where \tilde{G}_u stands for \tilde{G}_u^ϕ , \tilde{G}_{zz}^A , $\tilde{G}_{\phi\phi}^{Aa}$, $\tilde{G}_{\phi\phi}^{Ab}$, or $\tilde{G}_{\phi\phi}^{Ac}$.

Since in (13), all Bessel and Hankel functions are in the form of ratios, the possible overflow/underflow problems in the numerical calculations of special cylindrical functions in (15) can be avoided, and the efficiency can be improved. In order to further improve the efficiency and accuracy of (15), an envelope extraction method in [11, 12] with respect to n should be used to yield

$$\begin{aligned} \tilde{G}_u = & -\frac{1}{4\omega} \sum_{n=-\infty}^{\infty} \left\{ \left[\left(\frac{\partial^2}{k_{\rho_j}^2 \partial \rho \partial \rho'} \right)^q \left(H_n^{(2)}(k_{\rho_j} \rho) J_n(k_{\rho_j} \rho') \right) \right] \right. \\ & \cdot (n/k_{\rho_j})^p \cdot [f_u(n, k_z) - C_u(k_z)] e^{jn\Delta\phi} \left. \right\} \\ & -\frac{1}{4\omega} C_u(k_z) F_{1u} \left[H_0^{(2)}(k_{\rho_j} |\boldsymbol{\rho} - \boldsymbol{\rho}'|) \right] \end{aligned} \quad (16)$$

where $C_u(k_z)$ is the limit of $f_u(n, k_z)$ when $n \rightarrow \infty$. $F_{1u}[H_0^{(2)}(k_{\rho_j} |\boldsymbol{\rho} - \boldsymbol{\rho}'|)]$ corresponds to each component of \tilde{G}_u and is given by

$$\begin{aligned} F_1^\phi \left[H_0^{(2)}(k_{\rho_j} |\boldsymbol{\rho} - \boldsymbol{\rho}'|) \right] &= F_{1zz}^A \left[H_0^{(2)}(k_{\rho_j} |\boldsymbol{\rho} - \boldsymbol{\rho}'|) \right] = F_{1\phi\phi}^{Ac} \left[H_0^{(2)}(k_{\rho_j} |\boldsymbol{\rho} - \boldsymbol{\rho}'|) \right] \\ &= H_0^{(2)}(k_{\rho_j} |\boldsymbol{\rho} - \boldsymbol{\rho}'|) \end{aligned} \quad (17a)$$

$$F_{1\phi\phi}^{Aa} \left[H_0^{(2)}(k_{\rho_j} |\boldsymbol{\rho} - \boldsymbol{\rho}'|) \right] = \frac{\partial^2 H_0^{(2)}(k_{\rho_j} |\boldsymbol{\rho} - \boldsymbol{\rho}'|)}{k_{\rho_j}^2 \partial \phi \partial \phi'} \quad (17b)$$

$$F_{1\phi\phi}^{Ab} \left[H_0^{(2)}(k_{\rho_j} |\boldsymbol{\rho} - \boldsymbol{\rho}'|) \right] = \frac{\partial^2 H_0^{(2)}(k_{\rho_j} |\boldsymbol{\rho} - \boldsymbol{\rho}'|)}{k_{\rho_j}^2 \partial \rho \partial \rho'}. \quad (17c)$$

Apparently, from Equation (16), we find that the spectrum \tilde{G}_u will decay slowly at a small angle of $(\phi - \phi')$ due to the Hankel functions, when k_z tends to infinity. Thus another envelop extraction with respect

to k_z should be applied, according to [11, 12]. As a result, the spatial domain Green's function expression becomes

$$G_u = \frac{1}{2\pi} \int_{-\infty}^{\infty} \left(\tilde{G}_u + \frac{1}{4\omega} C_u(k_{z\infty}) F_{1u} \left[H_0^{(2)}(k_{\rho_j} |\boldsymbol{\rho} - \boldsymbol{\rho}'|) \right] \right) e^{-jk_z(z-z')} dk_z - \frac{j}{4\pi\omega} C_u(k_{z\infty}) F_{2u} \quad (18)$$

where G_u stands for G^ϕ , G_{zz}^A , $G_{\phi\phi}^{Aa}$, $G_{\phi\phi}^{Ab}$, or $G_{\phi\phi}^{Ac}$ and is the limit of $C_u(k_z)$ when $k_z \rightarrow \infty$. F_{2u} corresponds to each component of G_u and is given by

$$F_2^\phi = F_{2zz}^A = F_{2\phi\phi}^{Ac} = \frac{e^{-jk|\mathbf{r} - \mathbf{r}'|}}{|\mathbf{r} - \mathbf{r}'|} = \frac{-j}{2} \int_{-\infty}^{\infty} H_0^{(2)}(k_{\rho_j} |\boldsymbol{\rho} - \boldsymbol{\rho}'|) e^{-jk_z(z-z')} dk_z \quad (19a)$$

$$F_{2\phi\phi}^{Aa} = \frac{-j}{2} \int_{-\infty}^{\infty} \frac{1}{k_{\rho_j}^2} \frac{\partial^2}{\partial\phi\partial\phi'} H_0^{(2)}(k_{\rho_j} |\boldsymbol{\rho} - \boldsymbol{\rho}'|) e^{-jk_z(z-z')} dk_z \quad (19b)$$

$$F_{2\phi\phi}^{Ab} = \frac{-j}{2} \int_{-\infty}^{\infty} \frac{1}{k_{\rho_j}^2} \frac{\partial^2}{\partial\rho\partial\rho'} H_0^{(2)}(k_{\rho_j} |\boldsymbol{\rho} - \boldsymbol{\rho}'|) e^{-jk_z(z-z')} dk_z. \quad (19c)$$

The explicit expressions of (19b)–(19c) are presented as (A5a)–(A5b) in Appendix A.

After the quasistatic-wave part is extracted in (16), the remaining dynamic part can be approximated by the RFFM method, which was proposed in [22]. Thus, the following expression is obtained

$$\tilde{G}_u + \frac{1}{4\omega} C_u(k_{z\infty}) F_{1u} \left[H_0^{(2)}(k_{\rho_j} |\boldsymbol{\rho} - \boldsymbol{\rho}'|) \right] \cong \sum_{l=1}^{N_{sw}} \frac{a_l}{k_z^2 - k_{zl}^2} \quad (20)$$

where $-\pi < \arg\{k_{zl}\} \leq 0$ is enforced to ensure that the solution obtained for \tilde{G}_u fulfills the causality and radiation conditions [18].

Then, with the use of the following integral identity

$$\int_{-\infty}^{\infty} \frac{e^{-jk_z(z-z')}}{k_z^2 - k_{zl}^2} dk_z = -\pi j \frac{e^{-jk_{zl}(z-z')}}{k_{zl}} \quad (21)$$

the spatial domain MPGFs for cylindrically stratified media can be cast into a finite sum of quasistatic-wave and surface-wave contributions as

$$G_u \cong -\frac{j}{4\pi\omega} C_u(k_{z\infty}) F_{2u} - \frac{j}{2} \sum_{l=1}^{N_{sw}} a_l \frac{e^{-jk_{zl}(z-z')}}{k_{zl}}. \quad (22)$$

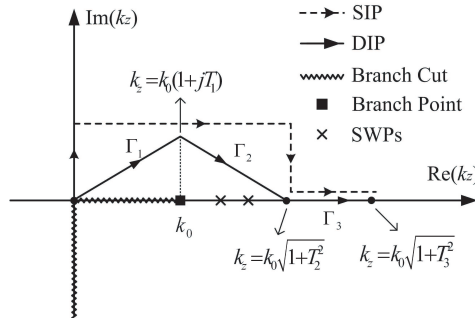


Figure 2. Sommerfeld integration path (SIP), deformed integration path (DIP) and possible singularities on the complex k_z plane.

In order to apply the RFFM method, the deformed integration path (DIP) is defined in Fig. 2, and the parameters are shown as [22]

$$\begin{aligned}
 \text{for } \Gamma_1: \quad k_z &= k_0(1 + jT_1) \frac{t_1}{T_1}, \quad 0 \leq t_1 < T_1, \\
 \text{for } \Gamma_2: \quad k_z &= k_0 \left[1 + jT_1 + \frac{(\sqrt{1 + T_2^2} - 1 - jT_1) t_2}{T_2 - T_1} \right], \quad (23) \\
 &0 \leq t_2 < T_2 - T_1, \\
 \text{for } \Gamma_3: \quad k_z &= k_0 \sqrt{1 + (t_3 + T_2)^2}, \quad 0 \leq t_3 < T_3 - T_2,
 \end{aligned}$$

where k_0 is the wavenumber of free space.

The DIP parameter T_2 should be chosen to ensure that $k_0 \sqrt{1 + T_2^2}$ is greater than the wavenumbers of all layers, according to [22], and T_3 should be large enough, as discussed in [13]. The value of T_1 should be carefully chosen to meet the justification for shifting the path from the physical poles and branch point, according to [22]. In this paper, $T_1 = 1e^{-3}$ suffices to obtain the accurate results for the calculation of the spatial-domain MPGFs. In addition, the number of sampling points and poles should be large enough to capture and describe the behavior of the spectrum.

Lastly, we find it useful to add a brief discussion on the axial line problem ($\rho = \rho'$ and $\phi = \phi'$). In this case, the $H_0^{(2)}(k_{\rho_j} |\rho - \rho'|)$ related terms in (16) are singular since the argument of the Hankel function is zero. Thus, (16) and (20) are not valid in the proposed RFFM method, and (22) can not be applied for obtaining the spatial domain MPGFs. To alleviate this problem, a hybrid method [23] or a small argument Hankel function approximation method [15] should be applied in the MoM-based algorithm.

2.1. Numerical Results and Discussions

In this section, numerical examples are presented to demonstrate the validity of the proposed method for calculating the spatial-domain MPGFs of a two layer structure when $\rho = \rho'$ and $\phi \neq \phi'$. All algorithms are programmed in Matlab and performed on a PC desktop computer with Intel (R) Core (TM) 2 Duo CPU 2.20 GHz.

Consider a two-layer structure, as shown in Fig. 1. The parameters that define the structure are as follows: Layer 1: $\varepsilon_{r1} = 2.0$, $\mu_{r1} = 1$. Layer 2: $\varepsilon_{r2} = 4.0$, $\mu_{r2} = 1$. $a_0 = 50$ mm, $a_1 = 52$ mm, $a_2 = \rho' = 54$ mm, $\rho = \rho'$, $\phi - \phi' = 0.2$. The operating frequency is $f = 6$ GHz. For the sake of convenience, we take the calculation of spatial-domain component $G_{\phi\phi}^A$ as an example, which can be expressed as

$$G_{\phi\phi}^A = G_{\phi\phi}^{Aa} + G_{\phi\phi}^{Ab} + G_{\phi\phi}^{Ac}. \quad (24)$$

The proposed RFFM method is applied on the DIP shown in Fig. 2. Fig. 3 shows results for $\tilde{G}_{\phi\phi}^A$ along the deformed path Γ_1 and Γ_2 of Fig. 2. It is noted that the values arising from the proposed RFFM method are in good agreement with the exact values of $\tilde{G}_{\phi\phi}^A$, and the maximum relative error between the two values is found to be below 0.06%. This maximum relative error is obtained by computing the relative error between the exact and the approximation values of $\tilde{G}_{\phi\phi}^A$ along the path Γ_1 and Γ_2 of Fig. 2. Please note that the exact values are obtained via (16), and the approximate values are obtained via (16) and (20).

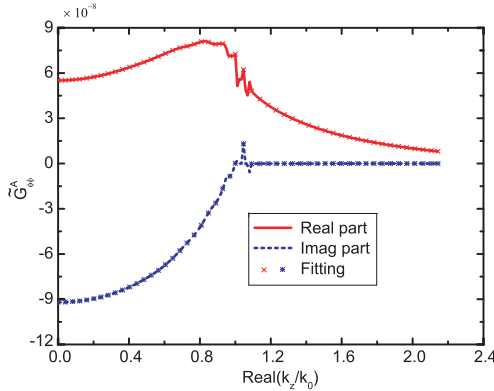


Figure 3. Real and imaginary parts of the spectral-domain Green's function $\tilde{G}_{\phi\phi}^A$ for the structure of Fig. 1 along the path Γ_1 and Γ_2 of Fig. 2. The exact results (solid and dashed line) are compared with those obtained via (16) and (20) ('x', '*').

In Table 1, we present results for the normalized poles and residues of $\tilde{G}_{\phi\phi}^A$ of Fig. 3 via (20), and we compare these values with the numerical exact results obtained by the contour integrals [25]. It is observed that the poles obtained by the proposed method coincide with the poles obtained by the method in [25] within six significant figures. The real part of the residues by the former method also coincide within three significant figures. It shows a good agreement between the two methods. On the other hand, the CPU time needed to obtain the poles and residues by the proposed method is about 14 seconds, which is much less than 30 seconds by the method in [25].

Due to the accurate approximation provided by the spectral-domain expression (16) and (20), we can conclude that the approximation provided by its spatial-domain counterpart (22) should also be very accurate. This is verified in Fig. 4 where the results for $G_{\phi\phi}^A$ obtained with the closed-form expression (22) are compared with results obtained via numerical integration of Sommerfeld integrals (exact). It is noted that the numerical integration method cannot be applied to the Sommerfeld integrals directly, since the spectral domain Green's functions are slowly convergent or even divergent. As discussed in [13], we use the following equation to obtain the exact results,

$$G_u = G_{\text{quasi}} + G_{\text{numer}} \tag{25}$$

where G_{quasi} stands for the quasi-static parts, and can be obtained by the same method in Section 2. G_{numer} stands for the integrals of the remaining spectral domain Green's functions after the quasi-static

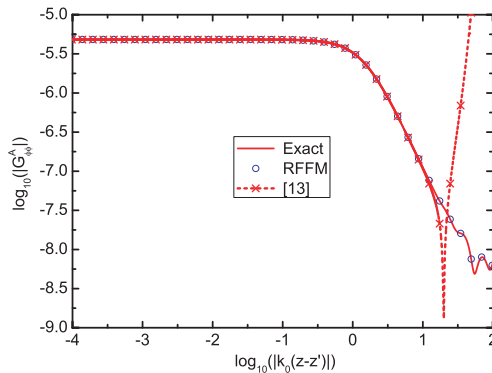


Figure 4. Magnitude of the spatial-domain Green's function $G_{\phi\phi}^A$ for the structure of Fig. 1. Exact integration results (solid line) are compared with those obtained via (22) and the three-level method proposed in [13] ('o', and dotted line with 'x').

Table 1. Normalized poles and residues of the spectral-domain Green's functions studied in Fig. 3. The results obtained by the proposed RFFM method are compared with the results obtained by using the exact expression via a numerical algorithm [25].

	[25]	Eqn. (20)		[25]	Eqn. (20)
k_{z1}/k_0	1.007017	1.007019	Res_1	-6.079×10^{-9}	$-6.088 \times 10^{-9} - j2.299 \times 10^{-11}$
k_{z2}/k_0	1.046748	1.046747	Res_2	-2.481×10^{-9}	$-2.483 \times 10^{-9} + j1.704 \times 10^{-12}$
k_{z3}/k_0	1.071425	1.071424	Res_3	1.080×10^{-9}	$1.080 \times 10^{-9} - j1.614 \times 10^{-12}$
k_{z4}/k_0	1.079684	1.079683	Res_4	1.213×10^{-9}	$1.214 \times 10^{-9} - j1.567 \times 10^{-12}$

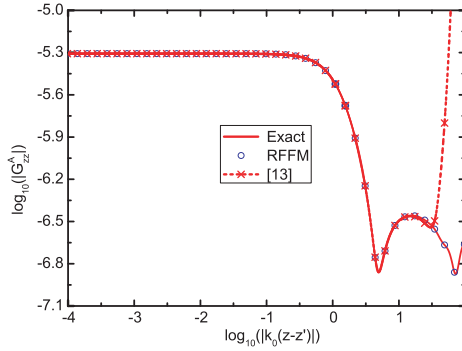


Figure 5. Magnitude of the spatial-domain Green's function G_{zz}^A for the structure of Fig. 1. Exact integration results (solid line) are compared with those obtained via (22) and the three-level method proposed in [13] ('o', and dotted line with 'x').

parts are extracted, and can be obtained via the Romberg integration method. Meanwhile, the integration path is the SIP shown in Fig. 2, and the relative error is selected with of 10^{-4} . In addition, the results obtained by the three-level method [13] is also demonstrated in Fig. 4. It is noted that the proposed RFFM method is quite successful and coincides perfectly with the results of the numerical integration, while the three-level method fails in fitting the far field. For the sake of completeness, the spatial domain components G_{zz}^A , and G^ϕ are also plotted in Figs. 5 and 6. From Figs. 5, 6, the same conclusions can be obtained. The relative errors between exact results and the approximate formulas of (22) for $G_{\phi\phi}^A$, G_{zz}^A , and G^ϕ are shown in Fig. 7, it is observed that the relative errors are all basically below 1%. The CPU time required by the proposed RFFM method is about 14s for

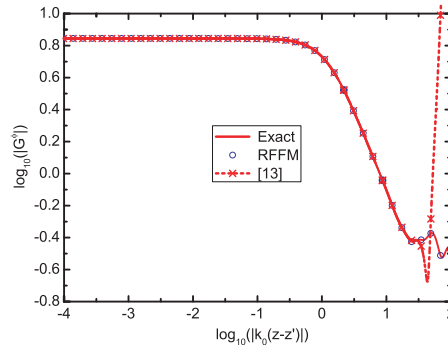


Figure 6. Magnitude of the spatial-domain Green’s function G^ϕ for the structure of Fig. 1. Exact integration results (solid line) are compared with those obtained via (22) and the three-level method proposed in [13] (‘o’, and dotted line with ‘x’).

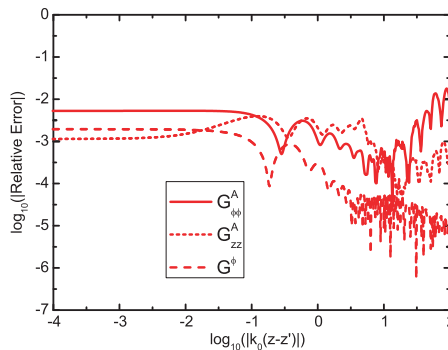


Figure 7. Relative errors of the spatial-domain Green’s functions $G_{\phi\phi}^A$, G_{zz}^A , and G^ϕ between the results calculated by the proposed RFFM method and the exact results.

each component, while the CPU time required by the exact numerical integration method is about 228s for each component.

For the sake of comparison, the parameters used in the proposed RFFM method for the structure of Fig. 1 are as follows: $T_1 = 0.001$, $T_2 = 1.9$, and $T_3 = 6$, number of samples are $M_1 = 100$, $M_2 = 600$, $M_3 = 2$, and number of rational functions is $N_{sw} = 30$; while the parameters used in the method [13] are as follows: $T_1 = 0.2$, $T_2 = 5$, and $T_3 = 7$, number of samples are $M_1 = 100$, $M_2 = 300$, and $M_3 = 2$. The number of harmonics is $N_h = 200$, and the number of samplings of each component of the spatial domain MPGFs is $N = 601$ for all the methods.

3. CONCLUSIONS

An efficient and fully numerical methodology for the computation of spatial-domain MPGFs in cylindrically stratified media has been presented. The RFFM method is applied for the approximation of spectral-domain MPGFs after the quasistatic-wave parts are extracted. Then the closed-form Green's functions are obtained with the use of integral identities, which can be applied in both the near- and far-field. Since the proposed methodology is fully automatic, analytical determination and extraction of surface wave poles of the spectrum are avoided prior to the fitting.

ACKNOWLEDGMENT

The authors thank Prof. G. Dural, Middle East Technical University, Ankara, Turkey, for providing reference [16].

APPENDIX A. SOME IDENTITIES

We define W_0 as follows

$$W_0 = \frac{e^{-jk|\mathbf{r}-\mathbf{r}'|}}{|\mathbf{r}-\mathbf{r}'|} = \frac{-j}{2} \int_{-\infty}^{\infty} H_0^{(2)}(k_{\rho_j} |\boldsymbol{\rho}-\boldsymbol{\rho}'|) e^{-jk_z(z-z')} dk_z \quad (\text{A1})$$

where

$$\begin{aligned} |\mathbf{r}-\mathbf{r}'| &= \sqrt{(z-z')^2 + \rho^2 + \rho'^2 - 2\rho\rho' \cos(\phi-\phi')} \\ |\boldsymbol{\rho}-\boldsymbol{\rho}'| &= \sqrt{\rho^2 + \rho'^2 - 2\rho\rho' \cos(\phi-\phi')}. \end{aligned}$$

It can be derived that

$$\begin{aligned} \frac{\partial^2}{\partial\phi\partial\phi'} H_0^{(2)}(k_{i\rho} |\boldsymbol{\rho}-\boldsymbol{\rho}'|) &= \left[\frac{\rho^2 \rho'^2 \sin^2(\phi-\phi')}{|\boldsymbol{\rho}-\boldsymbol{\rho}'|^2} H_0^{(2)}(k_{i\rho} |\boldsymbol{\rho}-\boldsymbol{\rho}'|) k_{i\rho}^2 \right. \\ &\quad \left. + \frac{\rho\rho'(\rho^2 + \rho'^2) \cos(\phi-\phi') - 2\rho^2 \rho'^2}{|\boldsymbol{\rho}-\boldsymbol{\rho}'|^3} k_{i\rho} H_1^{(2)}(k_{i\rho} |\boldsymbol{\rho}-\boldsymbol{\rho}'|) \right] \quad (\text{A2a}) \end{aligned}$$

$$\begin{aligned} \frac{\partial^2}{\partial\rho\partial\rho'} H_0^{(2)}(k_{i\rho} |\boldsymbol{\rho}-\boldsymbol{\rho}'|) &= \\ &= \left[\frac{2\rho\rho' - (\rho^2 + \rho'^2) \cos(\phi-\phi')}{|\boldsymbol{\rho}-\boldsymbol{\rho}'|^3} H_1^{(2)}(k_{i\rho} |\boldsymbol{\rho}-\boldsymbol{\rho}'|) k_{i\rho} \right. \\ &\quad \left. - \frac{[\rho - \rho' \cos(\phi-\phi')][\rho' - \rho \cos(\phi-\phi')]}{|\boldsymbol{\rho}-\boldsymbol{\rho}'|^2} H_0^{(2)}(k_{i\rho} |\boldsymbol{\rho}-\boldsymbol{\rho}'|) k_{i\rho}^2 \right]. \quad (\text{A2b}) \end{aligned}$$

Meanwhile, we define the following integral W_1

$$W_1 = -\frac{j}{2} \int_{-\infty}^{\infty} \frac{1}{k_{i\rho}} H_0^{(2)}(k_{i\rho} |\boldsymbol{\rho} - \boldsymbol{\rho}'|) e^{-jk_z(z-z')} dk_z. \quad (\text{A3})$$

According to the same method of (A-7a) in [13], the closed form solution to W_1 can be obtained

$$W_1 = -\frac{j e^{-jk_s |\mathbf{r}-\mathbf{r}'|}}{k_s |\boldsymbol{\rho} - \boldsymbol{\rho}'|}. \quad (\text{A4})$$

So the closed form solutions to (19b)–(19c) can be obtained with the help of (A1)–(A4)

$$\begin{aligned} F_{2\phi\phi}^{Aa} &= -\frac{j}{2} \int_{-\infty}^{\infty} \frac{1}{k_{i\rho}^2} \frac{\partial^2}{\partial\phi\partial\phi'} H_0^{(2)}(k_{i\rho} |\boldsymbol{\rho} - \boldsymbol{\rho}'|) e^{-jk_z(z-z')} dk_z \\ &= \frac{\rho^2 \rho'^2 \sin^2(\phi - \phi')}{|\boldsymbol{\rho} - \boldsymbol{\rho}'|^2} W_0 - \frac{(\rho^2 + \rho'^2) \rho \rho' \cos(\phi - \phi') - 2\rho^2 \rho'^2}{|\boldsymbol{\rho} - \boldsymbol{\rho}'|^3} W_1 \end{aligned} \quad (\text{A5a})$$

$$\begin{aligned} F_{2\phi\phi}^{Ab} &= -\frac{j}{2} \int_{-\infty}^{\infty} \frac{1}{k_{i\rho}^2} \frac{\partial^2}{\partial\rho\partial\rho'} H_0^{(2)}(k_{i\rho} |\boldsymbol{\rho} - \boldsymbol{\rho}'|) e^{-jk_z(z-z')} dk_z \\ &= -\frac{2\rho\rho' - (\rho^2 + \rho'^2) \cos(\phi - \phi')}{|\boldsymbol{\rho} - \boldsymbol{\rho}'|^3} W_1 \\ &= -\frac{[\rho - \rho' \cos(\phi - \phi')][\rho' - \rho \cos(\phi - \phi')]}{|\boldsymbol{\rho} - \boldsymbol{\rho}'|^2} W_0. \end{aligned} \quad (\text{A5b})$$

REFERENCES

1. Wang, Q. and Q. Q. He, “An arbitrary conformal array pattern synthesis method that includes mutual coupling and platform effects,” *Progress In Electromagnetics Research*, Vol. 110, 297–311, 2010.
2. Li, W.-T., Y.-Q. Hei, and X.-W. shi, “Pattern synthesis of conformal arrays by a modified particle swarm optimization,” *Progress In Electromagnetics Research*, Vol. 117, 237–252, 2011.
3. Wang, X., M. Zhang, and S.-J. Wang, “Practicability analysis and application of PBG structures on cylindrical conformal microstrip antenna and array,” *Progress In Electromagnetics Research*, Vol. 115, 495–507, 2011.
4. Bucinkas, J., L. Nickelson, and V. Sugurovas, “Microwave scattering and absorption by a multilayered lossy metamaterial — Glass cylinder,” *Progress In Electromagnetics Research*, Vol. 105, 103–118, 2010.

5. Yang, P., F. Yang, and Z.-P. Nie, "DOA estimation with subarray divided technique and interpolated esprit algorithm on a cylindrical conformal array antenna," *Progress In Electromagnetics Research*, Vol. 103, 201–216, 2010.
6. Hall, R. C., C. H. Thng, and D. C. Chang, "Mixed potential Green's functions for cylindrical microstrip structures," *IEEE Antennas Propagat. Soc. Int Symp.*, Vol. 4, 1776–1779, 1995.
7. Svezhentsev, A. Y. and G. A. E. Vandenbosch, "Mixed-potential Green's functions for sheet electric current over metal-dielectric cylindrical structure," *Journal of Electromagnetic Waves and Applications*, Vol. 16, No. 6, 813–835, 2002.
8. Svezhentsev, A. Y. and G. A. E. Vandenbosch, "Spatial Green's function singularity for sheet electric current over dielectric coated cylinder," *IEEE Trans. on Antennas and Propagat.*, Vol. 52, No. 2, 608–610, 2004.
9. Svezhentsev, A. Y. and G. A. E. Vandenbosch, "Efficient spatial domain moment method solution of cylindrical rectangular microstrip antennas," *IEE Proc. Microw. Antennas Propag.*, Vol. 153, No. 4, 376–384, 2006.
10. Svezhentsev, A. Y., "Mixed-potential Green's function of an axially symmetric sheet magnetic current on a circular cylindrical metal surface," *Progress In Electromagnetics Research*, Vol. 60, 245–264, 2006.
11. Sun, J., "Development of Green's functions and its application for cylindrically stratified media," Ph.D. Thesis, Department of Electrical and Computer Engineering, National University of Singapore, Singapore, 2004.
12. Sun, J., C.-F. Wang, J. L.-W. Li, and M.-S. Leong "Mixed potential spatial domain Green's functions in fast computational form for cylindrically stratified media," *Progress In Electromagnetics Research*, Vol. 45, 181–199, 2004.
13. Sun, J., C. F. Wang, L. W. Li, and M. S. Leong, "Further improvement for fast computation of mixed potential Green's functions for cylindrically stratified media," *IEEE Trans. on Antennas and Propagat.*, Vol. 52, No. 11, 3026–3036, 2004.
14. Tokgoz, C. and G. Dural, "Closed-form Green's functions for cylindrically stratified media," *IEEE Trans. on Microwave Theory and Tech.*, Vol. 48, No. 1, 40–49, 2000.
15. Karan, S., V. B. Erturk, and A. Altintas, "Closed-form Green's function representations in cylindrically stratified media for method of moments applications," *IEEE Antennas Propagat.*, Vol. 57, No. 4, 1158–1168, 2009.

16. Acar, R. C., "Numerically efficient analysis and design of conformal printed structures in cylindrically layered media," Ph.D. Thesis, Department of Electrical and Computer Engineering, Middle East Technical Univ., Ankara, Turkey, 2007.
17. Okhmatovski, V. I. and A. C. Cangellaris, "Evaluation of layered media Green's functions via rational function fitting," *IEEE Microw. Wireless Compon. Lett.*, Vol. 14, No. 1, 22–24, 2004.
18. Kourkoulos, V. N. and A. C. Cangellaris, "Accurate approximation of Green's functions in planar stratified media in terms of a finite sum of spherical and cylindrical waves," *IEEE Trans. on Antennas and Propagat.*, Vol. 54, No. 5, 1568–1576, 2006.
19. Polymeridis, A. G., T. V. Yioultis, and T. D. Tsiboukis, "A robust method for the computation of Green's functions in stratified media," *IEEE Trans. on Antennas and Propagat.*, Vol. 55, No. 7, 1963–1969, 2007.
20. Gustavsen, B. and A. Semlyen, "Rational approximation of frequency domain responses by vector fitting," *IEEE Trans. on Power Del.*, Vol. 14, No. 3, 1052–1061, 1999.
21. Gustavsen, B., "Improving the pole relocating properties of vector fitting," *IEEE Trans. on Power Del.*, Vol. 21, No. 3, 1587–1592, 2006.
22. Ye, L. F., F. Zhao, K. Xiao, and S. L. Chai, "A robust method for the computation of Green's functions in cylindrically stratified media," *IEEE Trans. on Antennas and Propagat.*, to be published.
23. Acar, R. C. and G. Dural, "Mutual coupling of printed elements on a cylindrically layered structure using closed-form Green's functions," *Progress In Electromagnetics Research*, Vol. 78, 103–127, 2008.
24. Akyuz, M. S., V. B. Erturk, and M. Kalfa, "Closed-form Green's function representations for mutual coupling calculations between apertures on a perfect electric conductor circular cylinder covered with dielectric layers," *IEEE Trans. on Antennas and Propagat.*, Vol. 59, No. 8, 3094–3098, 2011.
25. Wang, D. X., E. K. N. Yung, R. S. Chen, and J. Bao, "A new method for locating the poles of Green's functions in a lossless or lossy multilayered medium," *IEEE Trans. on Antennas and Propagat.*, Vol. 58, No. 7, 2295–2300, Jul. 2010.